



## Assembly Automation

CurviPicker: a continuum robot for pick-and-place tasks  
Zhixiong Yang, Bin Zhao, Liang Bo, Xiangyang Zhu, Kai Xu,

### Article information:

To cite this document:

Zhixiong Yang, Bin Zhao, Liang Bo, Xiangyang Zhu, Kai Xu, (2019) "CurviPicker: a continuum robot for pick-and-place tasks", Assembly Automation, <https://doi.org/10.1108/AA-12-2017-187>

Permanent link to this document:

<https://doi.org/10.1108/AA-12-2017-187>

Downloaded on: 06 June 2019, At: 07:04 (PT)

References: this document contains references to 31 other documents.

To copy this document: [permissions@emeraldinsight.com](mailto:permissions@emeraldinsight.com)

Access to this document was granted through an Emerald subscription provided by emerald-srm:367394 []

### For Authors

If you would like to write for this, or any other Emerald publication, then please use our Emerald for Authors service information about how to choose which publication to write for and submission guidelines are available for all. Please visit [www.emeraldinsight.com/authors](http://www.emeraldinsight.com/authors) for more information.

### About Emerald [www.emeraldinsight.com](http://www.emeraldinsight.com)

Emerald is a global publisher linking research and practice to the benefit of society. The company manages a portfolio of more than 290 journals and over 2,350 books and book series volumes, as well as providing an extensive range of online products and additional customer resources and services.

Emerald is both COUNTER 4 and TRANSFER compliant. The organization is a partner of the Committee on Publication Ethics (COPE) and also works with Portico and the LOCKSS initiative for digital archive preservation.

\*Related content and download information correct at time of download.

# CurviPicker: a continuum robot for pick-and-place tasks

Zhixiong Yang, Bin Zhao and Liang Bo

Shanghai Jiao Tong University – UM-SJTU Joint Institute, Shanghai, China, and

Xiangyang Zhu and Kai Xu

School of Mechanical Engineering, Shanghai Jiao Tong University, Shanghai, China

## Abstract

**Purpose** – Pick-and-place tasks are common across many industrial sectors, and many rigid-linked robots have been proposed for this application. This paper aims to alternatively present the development of a continuum robot for low-load medium-speed pick-and-place tasks.

**Design/methodology/approach** – An inversion of a previously proposed dual continuum mechanism, as a key design element, was used to realize the horizontal movements of the CurviPicker's end effector. A flexible shaft was inserted to realize rotation and translation about a vertical axis. The design concept, kinematics, system descriptions and proof-of-concept experimental characterizations are elaborated.

**Findings** – Experimental characterizations show that the CurviPicker can achieve satisfactory accuracy after motion calibration. The CurviPicker is easy to control due to its simple kinematics, while its structural compliance makes it safe to work with, as well as less sensitive to possible target picking position errors to avoid damaging itself or the to-be-picked objects.

**Research limitations/implications** – The vertical translation of the CurviPicker is currently realized by moving the flexible shaft. Insertion of the flexible shaft introduces possible disturbances. It is desired to explore other form of variations to use structural deformation to realize the vertical translation.

**Practical implications** – The proposed CurviPicker realizes the Schönflies motions via a simple structure. Such a robot can be used to increase robot presence and automation in small businesses for low-load medium-speed pick-and-place tasks.

**Originality/value** – To the best of the authors' knowledge, the CurviPicker is the first continuum robot designed and constructed for pick-and-place tasks. The originality stems from the concept, kinematics, development and proof-of-concept experimental characterizations of the CurviPicker.

**Keywords** Compliant mechanisms, Kinematics, Pick and place, CurviPicker, Delta robot

**Paper type** Research paper

## Nomenclature used in kinematics modeling

- $i$  = Index of the AS' backbones,  $i = 1, 2, 3, 4$ ;
- $r$  = Distance from the virtual central backbone to an AS's backbone;
- $\beta_i$  =  $\beta_i = (i - 1)\pi/2$  characterizes the division angle from the  $i^{\text{th}}$  backbone to the  $1^{\text{st}}$  backbone in the AS;
- $L$  = Length of the AS, the PS and the DS. Lengths of the AS and the PS shall be identical since the PS is assembled completely inside the AS. Lengths of the PS and the DS are set identical in this study even though they could be different in a general case;
- $L_i$  = Length of the AS's  $i^{\text{th}}$  backbone;
- $d$  = Diameter of the backbones;
- $q_i$  = Push-pull actuation of the AS's  $i^{\text{th}}$  backbone;  $q_i \equiv L_i - L$ ;
- $\theta$  = Bending angle of the AS, the PS and the DS;
- $\delta_i$  = A right-handed rotation angle from  $\hat{\mathbf{y}}_1$  about  $\hat{\mathbf{z}}_b$  to a ray passing through the central and the  $i^{\text{th}}$  backbone;
- $\delta$  =  $\delta \equiv \delta_1$  and  $\delta_i = \delta + \beta_i$ ;
- $D$  = Length of the straight multi-lumen guiding tube;

- $h$  = Translation of the end effector from the DS's end ring;
- $\varphi$  = Rotation of the end effector with respect to the DS's end ring;
- $\psi = \psi [\theta \ \delta \ \varphi \ h]^T$  is a configuration vector of the CurviPicker; and
- ${}^1\mathbf{R}_2$  = Coordinate transformation matrix from frame 2 to frame 1.

## 1. Introduction

Pick-and-place tasks, which can be achieved by Schönflies motions (three translations and one rotation about a vertical axis), are very common in production lines across many industrial sectors. These pick-and-place tasks, which were once carried out by SCARA (Selective Compliant Assembly Robot Arm) robots, were revolutionized by Delta parallel robots. A Delta robot possesses three parallelograms to achieve pure translations for the end effector, while the actuators' base mounting and the low-mass parallel structure enables the rapid movements (Clavel, 1990).

The current issue and full text archive of this journal is available on Emerald Insight at: [www.emeraldinsight.com/0144-5154.htm](http://www.emeraldinsight.com/0144-5154.htm)



Assembly Automation  
© Emerald Publishing Limited [ISSN 0144-5154]  
[DOI 10.1108/AA-12-2017-187]

*Research funding:* This work was supported in part by the National Natural Science Foundation of China (Grant No. 91648103, Grant No. 51722507 and Grant No. 51435010), and in part by the National Key R&D Program of China (Grant No. 2017YFC0110800).

Received 27 December 2017

Revised 24 July 2018

Accepted 22 August 2018

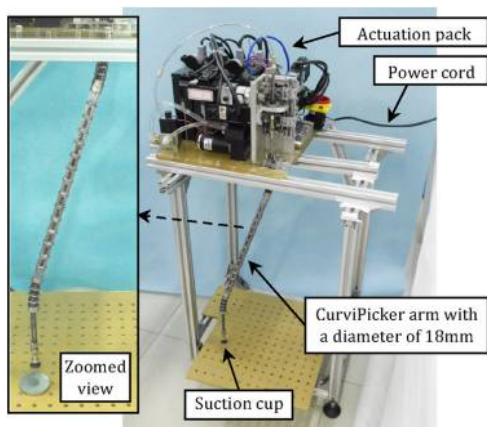
Then research activities on Delta robots thrived, spanning kinematic calibration (Vischer and Clavel, 1998), singularity analysis (Di Gregorio, 2004), structural optimizations (Miller, 2004; Zhang and Song, 2011), motion isotropy (Carricato, 2005), dimensional synthesis (Zhang et al., 2012) and form variations (Stock and Miller, 2003; Pernette et al., 1997). The H4 and Par4 parallel robots with articulated moving platforms were introduced to avoid the use of a central leg for improved performances in high-load high-acceleration applications (Pierrot and Company, 1999; Pierrot et al., 2009). Other parallel robots that could realize Schönflies motions include the McGill SMG robot (Angeles et al., 2006), the Quadruperon robot (Richard et al., 2006), the Heli4 robot (Krut et al., 2006), the Isoglide4 robot (Gogu, 2007), the 4-PRP<sub>a</sub>R robot (Li et al., 2013) and the Ragnar robot (Wu et al., 2015).

For a pick-and-place robot, not only efficiency and speed but also other factors, such as cost, safety and ease of use, should be considered. Possibly providing an alternative solution, this paper proposes the CurviPicker, the first continuum robot to realize the Schönflies motions via the use of four actuators, specifically design for low-load medium-speed pick-and-place tasks in a safe and affordable way.

Such pick-and-place tasks (e.g. placing tea bags or candy bars into a package tray) commonly exist in small businesses. These tasks are currently often carried out manually as the aforementioned SCARA or Delta robots with an excessive positioning accuracy may financially overburden these small businesses. As indicated by the experimental results in Section 5.2, the CurviPicker can operate at a speed that is equivalent to a CPM (Cycle per Minute) number of 60, with a load of up to 100 grams. In such scenarios with similar loads and throughputs, the CurviPicker can become a viable option for automation.

The CurviPicker in Figure 1 would be shown easy to control due to its simple kinematics. Its structural compliance makes it safe to work with, as well as more adaptable and less sensitive to possible picking position errors from trajectory planning to avoid damaging itself or to-be-picked objects. The CurviPicker may be used to increase robot presence and automation in small businesses for low-load medium-speed pick-and-place tasks. The design concept, kinematics, development and proof-of-concept experiments hence form this paper's main contributions.

**Figure 1** The constructed CurviPicker, a continuum pick-and-place robot



The CurviPicker is a continuum robot and the researches on continuum robots attracted lots of attentions in the past decades due to their light weights, design compactness, inherent safety, etc. (Trivedi et al., 2008; Walker, 2013; Burgner-Kahrs et al., 2015). The continuum robots may seem inherently inaccurate and have poor payload capacity. However, for the low-load pick-and-place tasks where moderate positioning accuracy is acceptable, the safety and affordability features of the CurviPicker can truly stand out. For example, as indicated by the collision tests in Section 5.3, the CurviPicker's arm can be completely stopped by an external obstacle. When the obstacle is removed, the CurviPicker immediately returns to normal without requiring re-conditioning the system. These features may help the CurviPicker fulfill the demands from small businesses for safe and affordable automation.

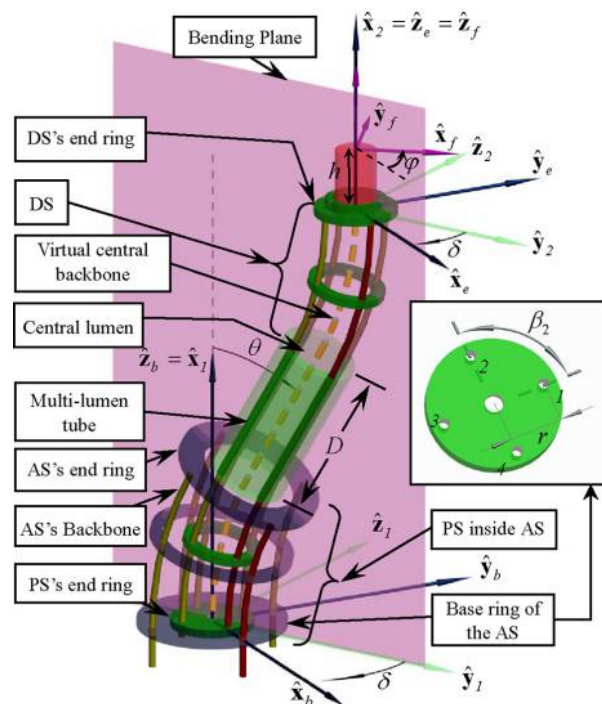
This paper is organized as follows. Section 2 explains the design concept. With the kinematics and structural optimization presented in Section 3, Section 4 describes the system components in detail. Section 5 presents the actuation calibration and the experimental characterizations of the CurviPicker, while the conclusions and the future work are summarized in Section 6.

## 2. Design concept

It is critical to realize the Schönflies motions in a simple and effective way for a pick-and-place robot. The CurviPicker's key functional structure for translations is inspired by the dual continuum mechanism that was used in a surgical robot (Xu et al., 2015).

A one-stage dual continuum mechanism as shown in Figure 2 consists of a distal segment (DS), a multi-lumen tube

**Figure 2** Nomenclature and coordinates of the CurviPicker: numbers in the inset indicate the index of the backbones of the AS



and a proximal segment (PS). The segments are structurally similar. Each segment consists of a base ring, several spacer rings, an end ring and several backbones. The backbones are thin super-elastic nitinol rods and could undergo both stretching and compressive loads. For this reason they are not addressed as tendons that are used in (Li and Du, 2013; Li et al., 2016). The backbones are attached to the end ring and can slide in the holes of the base and the spacer rings. When the backbones of the DS and the PS are connected, bending the PS bends the DS in the opposite direction.

In the previous use, the multi-lumen tube is stationary (Xu et al., 2015). An inversion of the dual continuum mechanism is created by grounding the PS's end ring as shown in Figure 2. When the DS is identical to the PS, their bending would also be identical in an ideal case. This would lead to translational movements of the DS's end ring, when the PS's end ring is attached to the ground.

An actuation segment (AS), which is structurally similar to the DS or PS, is used to bend the PS. In Figure 2, the AS's end ring is attached to the PS's base ring. The AS is bent by pushing and pulling its four backbones. Then the PS is bent and bending of the DS is also generated.

The proposed design concept could seem similar to flexure parallelograms that are widely used. But the output of a flexure parallelogram is usually planar and limited. The design could also be seen similar to the prominent elephant trunk robots (Hannan and Walker, 2003; Yang et al., 2006). The main difference is that two coupled segments are involved in the CurviPicker to generate pure translations of the end effector, whereas the segments are individually actuated in the aforementioned continuum manipulators.

The inverted dual continuum mechanism realizes 2-DoF translational movements. A flexible shaft can be inserted into the central lumen of the dual continuum mechanism to realize a third translation and a rotation in and about the vertical axis. Then all the desired movements of the CurviPicker for pick-and-place tasks can be generated.

### 3. Kinematics and structural optimization

Core structure of the CurviPicker is the inverted dual continuum mechanism as in Figure 2. It consists of a DS, a PS and a number of straight guiding lumens, whereas the PS is actuated by an AS. The kinematics is based on the assumption that each segment bends into circular shapes. This assumption was widely adopted (Xu and Simaan, 2008; Webster and Jones, 2010) and experimentally verified (Xu and Simaan, 2008; Xu et al., 2014).

Only kinematics analysis is presented in this paper for the proof of concept. Dynamics modeling for vibration suppression is deferred to a future study for improving the performances.

#### 3.1 Nomenclatures and coordinate systems

Nomenclatures are defined in Nomenclature used in kinematics modeling, while five coordinate systems are defined as follows:

- The XY plane of the *Base Coordinate*  $\{b\} \equiv \{\hat{\mathbf{x}}_b, \hat{\mathbf{y}}_b, \hat{\mathbf{z}}_b\}$  is aligned with the AS's base ring with the origin at the ring's center.  $\hat{\mathbf{x}}_b$  points from the origin to the first backbone. The backbone numbering could be referred to the definition of  $\delta_i$ . The AS's base ring coincides with the PS's end ring.

- *Bending Plane Coordinate-1*  $\{1\} \equiv \{\hat{\mathbf{x}}_1, \hat{\mathbf{y}}_1, \hat{\mathbf{z}}_1\}$  shares its origin with  $\{b\}$ . The entire structure, including the AS, the PS and the DS, bends in the XY plane of  $\{1\}$ .
- *Bending Plane Coordinate-2*  $\{2\} \equiv \{\hat{\mathbf{x}}_2, \hat{\mathbf{y}}_2, \hat{\mathbf{z}}_2\}$  is translated from  $\{1\}$  such that the origin is moved to the center of the DS's end ring.
- *End Ring Coordinate*  $\{e\} \equiv \{\hat{\mathbf{x}}_e, \hat{\mathbf{y}}_e, \hat{\mathbf{z}}_e\}$  is fixed to the DS's end ring.  $\hat{\mathbf{x}}_e$  points from the ring's center to the first backbone. Since the DS and the PS are structurally identical, their identical bending patterns maintain the identical orientations between  $\{1\}$  and  $\{2\}$ ,  $\{b\}$  and  $\{e\}$ , respectively.
- *End Effector Coordinate*  $\{f\} \equiv \{\hat{\mathbf{x}}_f, \hat{\mathbf{y}}_f, \hat{\mathbf{z}}_f\}$  is translated from  $\{e\}$  along  $\hat{\mathbf{z}}_e$  with a rotation about  $\hat{\mathbf{z}}_e$ .

#### 3.2 Kinematics

All the segments (DS, PS and AS) bend into circular arcs. A virtual central backbone (the dashed line in Figure 2) characterizes the length and the shape of each segment.

Movements of the DS's end ring would be translational due to the identical bending of the DS and the PS. The homogeneous transformation matrix linking  $\{b\}$  and  $\{e\}$  is written as in equation (1) due to the fact that the DS's end ring is translated from the PS's end ring following a path in the bending plane.

The upper left corner of  ${}^b\mathbf{T}_e$  is an identity matrix  $\mathbf{I}_{3 \times 3}$  since the DS's end ring is purely translated. The translation follows a path in the bending plane sequentially along:

- The PS's central backbone (a circular arc of length  $L$  and bent angle  $\theta$ );
- The axis of the multi-lumen tube for a distance of  $D$ ; and
- The DS's central backbone (again a circular arc of length  $L$  and bent angle  $\theta$ ).

As the bending plane is characterized by  $\delta$ , the expression of  ${}^b\mathbf{p}_e$  is hence derived as in equation (2):

$${}^b\mathbf{T}_e = \begin{bmatrix} \mathbf{I}_{3 \times 3} & {}^b\mathbf{p}_e \\ 0 & 1 \end{bmatrix} \quad (1)$$

$${}^b\mathbf{p}_e = \begin{bmatrix} 2L(1 - \cos\theta)\cos\delta/\theta + D\sin\theta\cos\delta \\ 2L(\cos\theta - 1)\sin\delta/\theta - D\sin\theta\sin\delta \\ 2L\sin\theta/\theta + D\cos\theta \end{bmatrix} \quad (2)$$

where  ${}^b\mathbf{p}_e = [0 \ 0 \ 2L + D]^T$  when  $\theta \rightarrow 0$ . The expression of  ${}^b\mathbf{p}_e$  is obtained using the Taylor series of  $\sin\theta$  and  $\cos\theta$  as  $\theta$  approaches zero.

Please note that gravity or external loads may generate shape discrepancy between the DS and the PS of the CurviPicker (a.k.a. non-identical bending), and hence affect the positioning accuracy of the end effector. However, attempting to model this gravity/load dependent bending discrepancy may substantially increase the complexity of the model. While keeping the load low and implementing the simple kinematics of the CurviPicker, the motion calibration in Section 5.1 in fact lumped such bending discrepancy between the DS and the PS into the parameters of the actuation compensation.

A flexible shaft is inserted inside the DS and the PS to realize a translation and a rotation about  $\hat{\mathbf{z}}_e$ . Then the homogeneous transformation matrix linking  $\{e\}$  and  $\{f\}$  can be written as in

equation (3). Then the position and orientation of the end effector can be described by equation (4):

$${}^e\mathbf{T}_f = \begin{bmatrix} \cos\varphi & -\sin\varphi & 0 & 0 \\ \sin\varphi & \cos\varphi & 0 & 0 \\ 0 & 0 & 1 & h \\ 0 & 0 & 0 & 1 \end{bmatrix} \quad (3)$$

$${}^b\mathbf{T}_f = {}^b\mathbf{T}_e {}^e\mathbf{T}_f \quad (4)$$

The equation (4) represents the direct kinematics from the configuration space to the task space. However, analytic expressions for the inverse kinematics do not exist. The inverse kinematics from the task space to the configuration space has to be solved numerically.

Four backbones are pushed and pulled to bend the AS. With the PS assembled inside the AS, the AS and the PS would possess the same shape (the same  $\theta$  and  $\delta$  values), leading to coupled bending of the DS. Then actuation of the CurviPicker only concerns the push-pull lengths of the backbones in the AS.

The AS's length is related to that of the  $i^{\text{th}}$  backbone as in equation (5), with details available in (Xu and Simaan, 2008). Hence, the backbone actuation is in equation (6), following the definition of  $q_i$ :

$$L_i = L - r\theta\cos(\delta + \beta_i) \quad (5)$$

$$q_i = -r\theta\cos(\delta + \beta_i) \quad (6)$$

$$\mathbf{J}_{v\psi} = \begin{bmatrix} \frac{2L(c_\theta - 1)c_\delta}{\theta^2} + \frac{2Ls_\theta c_\delta}{\theta} + Dc_\theta c_\delta & \frac{2L(c_\theta - 1)s_\delta}{\theta} - Ds_\theta s_\delta & 0 & 0 \\ \frac{2L(1 - c_\theta)s_\delta}{\theta^2} - \frac{2Ls_\theta s_\delta}{\theta} - Dc_\theta s_\delta & \frac{2L(c_\theta - 1)c_\delta}{\theta} - Ds_\theta c_\delta & 0 & 0 \\ -\frac{2Ls_\theta}{\theta^2} + \frac{2Lc_\theta}{\theta} - Ds_\theta & 0 & 0 & 1 \end{bmatrix} \quad (10)$$

$$\mathbf{J}_{\omega\psi} = \begin{bmatrix} 0 & 0 & 0 & 0 \\ 0 & 0 & 0 & 0 \\ 0 & 0 & 1 & 0 \end{bmatrix} \quad (11)$$

where  $s_\theta$  and  $c_\theta$  stand for  $\sin\theta$  and  $\cos\theta$  respectively.

Expressions (12) are obtained from equation (6). Then  $\mathbf{J}_{\psi\mathbf{q}}$  can be derived as in equation (13), solving for  $\Delta\theta$  and  $\Delta\delta$  from equation (12):

$$\begin{cases} \Delta q_1 = -r\cos\delta \cdot \Delta\theta + r\theta\sin\delta \cdot \Delta\delta \\ \Delta q_2 = r\sin\delta \cdot \Delta\theta + r\theta\cos\delta \cdot \Delta\delta \end{cases} \quad (12)$$

$$\mathbf{J}_{\psi\mathbf{q}} = \begin{bmatrix} -\cos\delta/r & \sin\delta/r & 0 & 0 \\ \sin\delta/r\theta & \cos\delta/r\theta & 0 & 0 \\ 0 & 0 & 1 & 0 \\ 0 & 0 & 0 & 1 \end{bmatrix} \quad (13)$$

According to the defined  $\beta_i$  in Nomenclature used in kinematics modeling,  $q_1 = -q_3$  while  $q_2 = -q_4$ . Then the relations are derived as in equation (7) from equation (6):

$$\begin{cases} \theta = \sqrt{q_1^2 + q_2^2}/r \\ \delta = \text{atan}2(q_2, -q_1) \end{cases} \quad (7)$$

The configuration space of the CurviPicker is specified by  $\Psi = [\theta \ \delta \ \varphi \ h]^T$ , whereas the actuator space is specified by  $\mathbf{q} = [q_1 \ q_2 \ \varphi \ h]^T$ . The Jacobian matrix relating the actuator space and the task space could be derived as in equation (8):

$${}^b\dot{\mathbf{x}} = \mathbf{J}_{x\psi}\dot{\Psi} = \mathbf{J}_{x\psi}\mathbf{J}_{\psi\mathbf{q}}\dot{\mathbf{q}} \quad (8)$$

where  $\mathbf{J}_{x\psi}$  and  $\mathbf{J}_{\psi\mathbf{q}}$  are derived from equations (4) and (6), respectively, as follows.

$\mathbf{J}_{x\psi}$  is obtained by deriving the linear velocity Jacobian and the angular velocity Jacobian matrices separately as in equation (9).  $\mathbf{J}_{v\psi}$  is obtained by differentiating the position vector from equation (4) with respect to the configuration variables  $\Psi = [\theta \ \delta \ \varphi \ h]^T$  as in equation (10), while  $\mathbf{J}_{\omega\psi}$  is written directly since the only rotatable component is the central flexible shaft (the inverted dual continuum mechanism does not twist):

$$\mathbf{J}_{x\psi} = \begin{bmatrix} \mathbf{J}_{v\psi} \\ \mathbf{J}_{\omega\psi} \end{bmatrix} \quad (9)$$

Please note that  $\mathbf{J}_{\psi\mathbf{q}}$  is currently expressed in terms of  $\theta$  and  $\delta$ . It has an equivalent form in terms of  $q_1$  and  $q_2$  with equation (7) substituted into equation (13).

### 3.3 Structural optimization

Following the concept in Section 2 and the kinematics in Section 3.2, the CurviPicker design is finalized based on the structural optimization presented here.

Due to the CurviPicker's deforming pattern, its reachable workspace has a cylindrical shape. The reach in the radial direction could be written as in equation (14):

$$C = 2L(1 - \cos\theta)/\theta + D\sin\theta \quad (14)$$

If the CurviPicker is expected to have a workspace with a diameter of 300 mm,  $C$  shall be equal to 150 mm. For a quick pick-and-place robot, it is desired that small amount of actuation could move the end effector across the workspace. According to the actuation kinematics in equation (6), a

smaller  $\theta$  leads to smaller actuation lengths  $q_i$ . Hence, it is desired that the  $\theta$  value is small when  $C$  reaches 150 mm. obviously the longer the CurviPicker is, the smaller  $\theta$  value it should have to reach the same  $C$  value. Hence, a structural constraint is set in equation (15), limiting the CurviPicker's total length. The total length is not set too long with a consideration of limiting possible vibrations:

$$2L + D = 400 \text{ mm} \quad (15)$$

During the CurviPicker's intended operations, the backbones all undergo cyclic elastic deformations. According an existing study where thin nitinol wires were tested for fatigue behaviors (Tobushi et al., 2009), the maximal strain is 0.7 per cent to 0.8 per cent for  $10^6$  cycles with a loading frequency of 8.33 Hz (500 cycles per minute). Then a constraint on the bending strain is hence formulated in equation (16):

$$d/2R \leq 0.7\% \quad (16)$$

where  $R = L/\theta$  is the bending radius of the segments.

Replacing  $D$  in equation (14) with an expression of  $L$  using equation (15) and Substituting equation (14) with  $C = 150$  mm into equation (16) leads to the solved constraint on  $L$  as in equation (17):

$$L \geq 36.39 \text{ mm} \quad (17)$$

Then  $L$  is rounded to 40 mm due to the practical challenge of keeping  $L$  to an exact value while assembling the CurviPicker.  $L$  is listed in Table I together with other structural parameters.

It should be noted that a parasite translation of the DS's end ring in the  $\hat{z}_b$  direction is always associated with the segments' bending as a function of  $\theta$  as in equation (18).  $\Delta H$  increases with  $\theta$  and reaches the maximum when  $C$  in equation (14) reaches 150 mm. It can be clearly seen from equation (18) that setting  $L$  at 40mm also reduces this undesired translation. What's more, a shorter segment possesses higher elastic potential energy under the same amount of bending. As indicated in (Xu and Simaan, 2008), gravity can be neglected when the elastic potential energy of a continuum robot outnumbers the gravitational potential energy. Hence setting  $L$  at a smaller value helps reduce the influences of gravity:

$$\Delta H = 2L(1 - \sin\theta/\theta) + D(1 - \cos\theta) \quad (18)$$

Using the parameters listed in Table I, the CurviPicker's workspace can be generated by scanning its configuration space and visualized as in Figure 3.

#### 4. System descriptions

The CurviPicker was constructed as shown in Figure 1, following the design concept introduced in Section 2 and implementing results of the kinematics analysis in Section 3. The CurviPicker system shown in Figure 4 consists of the CurviPicker arm, the

**Table I** Structure parameters of the CurviPicker's arm

$\theta \in [0, 2\pi/15]$	$\delta \in [-\pi, \pi]$	$r = 8 \text{ mm}$
$L = 40 \text{ mm}$	$D = 320 \text{ mm}$	$h \in [110, 170 \text{ mm}]$
		$\varphi \in [-\pi, \pi]$

**Figure 3** Workspace of the CurviPicker

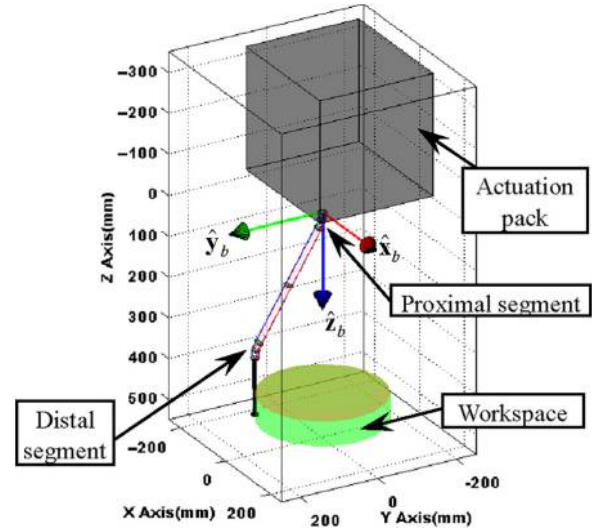
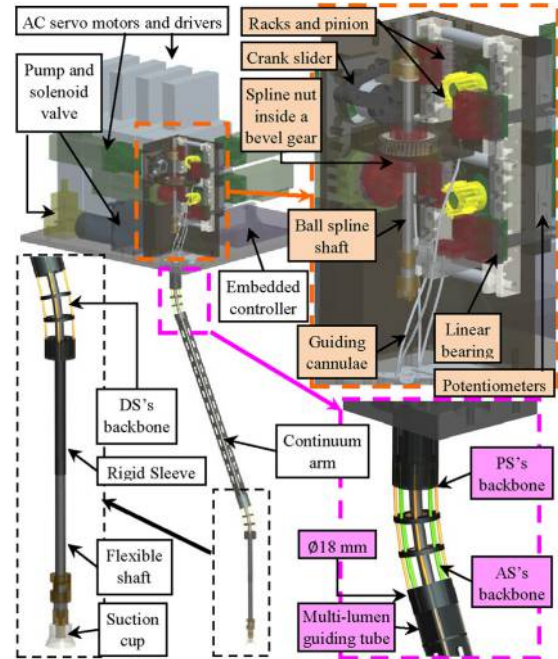


**Figure 4** The CurviPicker and its continuum arm



actuation assembly, a pump with solenoid valve, four AC servomotors with digital drivers and an embedded controller. The arm and the controller infrastructure are described in detail.

##### 4.1 The continuum arm and its actuation

The Curvipicker's motions are realized by the deformations of its continuum arm together with the translation/rotation of the central flexible shaft. The arm is shown in Figure 4 and its weight is about 200 grams.

The arm has an outer diameter of 18 mm. The PS and the DS share four backbones. The backbones of the PS and the DS pass through a rigid multi-lumen guiding tube. The backbones

could slide inside the lumens. The AS's backbones are arranged between the PS's backbones. All backbones have a diameter of 1.2 mm and are arranged on a  $\varnothing 16$  mm circle. The AS's backbones are pushed and pulled by the actuation assembly.

A hollow flexible shaft is assembled inside the central lumen of the CurviPicker's arm. The shaft can be translated and rotated. A suction cup is assembled to the distal end of the shaft via a fitting for picking up and placing down workpieces. The reason for selecting a suction cup mainly includes its versatility and action agility. The translation of the flexible shaft should be vertically downwards. A tube as a sleeve is attached to the DS's end ring to guide the shaft's translation.

Four AC servomotors (ISMH1-10B30CB from Inovance Inc., Shenzhen, China) are used to drive the CurviPicker's arm. Two servomotors drive the AS's backbones. According to the actuation kinematics in equation (6) with the  $\beta_i$ 's definition in Nomenclature used in kinematics modeling,  $q_1 = -q_3$  while  $q_2 = -q_4$ . And one pinion meshed with two gear racks generates such opposite translational outputs. The gear racks are attached to the sliders on two linear bearings. The AS's backbones are routed to the sliders via the guiding cannulae such that the pinions' rotations lead to the push/pull actuation of the backbones. The pinion is attached to the AC servomotor through a gearhead (YT401-20L from Yintong Inc., Shanghai, China) with a gear reduction ratio of 20:1. Two potentiometers are included to sense the absolute positions of the sliders.

The actuation assembly also realizes the translation and rotation of the flexible shaft. The flexible shaft is connected with a ball spline shaft. The spline shaft can translate freely inside a ball spline nut, whereas rotating the spline nut also rotates the spline shaft. The spline shaft is connected with two serially pinned links. These components essentially form a crank-slider mechanism for translations of the spline shaft. The crank is attached to the output shaft of the third servomotor's gearhead. The gear reduction ratio of this gearhead is 8:1.

The spline nut is attached inside a bevel gear such that rotation of the spline nut could be realized by another bevel gear that is driven by the 4th servomotor.

The spline shaft also has a central lumen that is used for airflows for the suction of various workpieces.

The selected spline shaft has an outer diameter of 6 mm and an effective travel of 70 mm. The motion range on the translational joint (the  $h$  value in Figure 2) is hence set to 60 mm (from 110 mm to 170 mm), as shown in Table I.

#### 4.2 Control infrastructure

The CurviPicker's control infrastructure is designed for repetitive pick-and-place tasks.

The four servomotors are driven by four digital drivers (IS620PS1R6I from Inovance Inc., Shenzhen, China). The digital driver could be accessed via the CAN (Controller Area Network) bus using the standard CANOpen protocol. It runs a one-millisecond servo loop and provides necessary low-level functions such as A/D conversion and interpolation.

The embedded controller is the Apalis T30 from Toradex AG, Switzerland. It has a 1.3 GHz multi-core CPU, 1 GByte RAM, and a wide spectrum of I/O interfaces including two channels of CAN communication. The operating system is the embedded Linux based on Linux for Tegra.

The suction cup is enabled by the vacuum pump (V985250DC24 from Pengpu Fluid Tech Co. Ltd, Shanghai, China) with a flow capacity of 9.5 L/min and controlled by a solenoid valve (VT317V from SMC Corp., Japan).

The total cost of the CurviPicker is about US\$3560, including US\$1800 for the four servomotors with the gearheads and their drivers, US\$370 for the embedded controller, US\$130 for the pump and the valves, US\$60 for the power supply and US\$1,200 for the raw materials, machining and aluminum profiles. It can be seen that a majority of the CurviPicker's cost is for the servomotors, the raw materials and the machining. If the CurviPicker is produced for a larger quantity, the unit cost will be driven considerably lower.

## 5. Experimental characterizations

Three sets of experiments were carried out on the CurviPicker to gauge its specifications and demonstrate its features and capabilities.

### 5.1 Motion calibration and repeatability tests

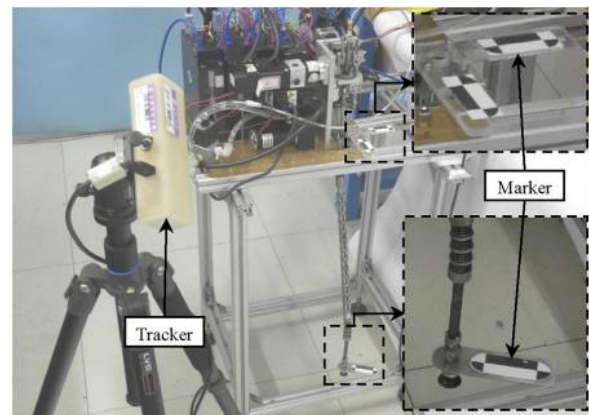
According to the existing studies (Xu and Simaan, 2006; Xu et al., 2015), there often exists a difference between a segment's actual bending angle and the assumed one. Hence, motion calibration is necessary for the CurviPicker to reach desired positions for pick-and-place tasks.

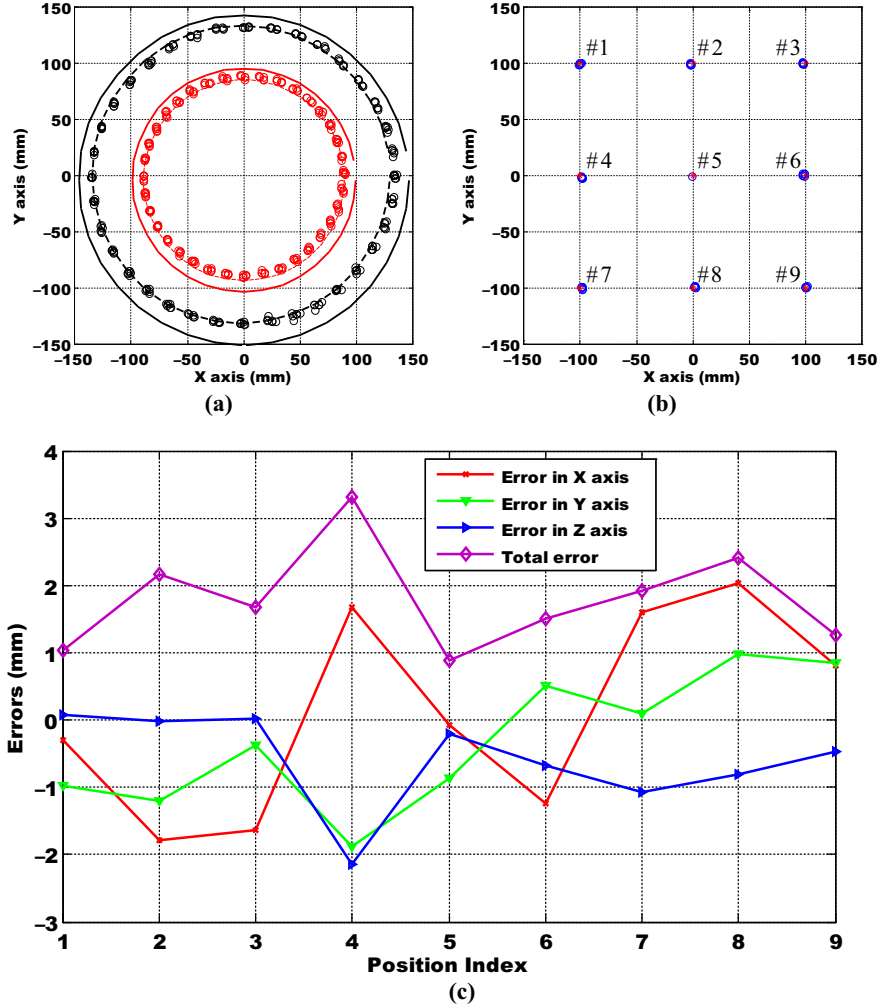
The CurviPicker was instructed to reach 72 positions on two circles inside its cylindrical workspace as shown in Figure 6 (a). The 72 positions correspond to the  $\theta$  values at  $4\pi/45$  ( $16^\circ$ ) and  $2\pi/15$  ( $24^\circ$ ) with the  $\delta$  value varying from  $-\pi$  to  $\pi$  ascendingly and then descendingly for three times in increments of  $\pi/18$  ( $10^\circ$ ). The  $h$  is set at 110 mm while the  $\varphi$  is set to 0.

As shown in Figure 5, two perpendicularly placed markers were attached near the base of the CurviPicker. They were used to form an intermediate coordinate system to quantify the position and orientation of the CurviPicker's tip. This intermediate coordinate has a known displacement from  $\{b\}$ . A third marker is attached to the end effector of the CurviPicker. Positions and orientations of the markers were read by an optical tracker (Micron Tracker SX60 from Claron Technology Inc.).

Actual positions of the CurviPicker's tip are plotted in Figure 6(a), indicated by the black and red round dots. The solid

Figure 5 Experimental setup for motion calibration



**Figure 6** Positioning errors of the CurviPicker (a) before and (b) after calibration with (c) the detailed errors at the designated nine positions

black and red circles indicate the desired radius that the tip should reach when the  $\theta$  is set to  $2\pi/15$  ( $24^\circ$ ) and  $4\pi/45$  ( $16^\circ$ ). It is clear that discrepancy exists between the ideal and the actual positions (the CurviPicker deforms less than the desired pose).

The errors on  $\delta$  were firstly examined. They were found to be between  $\pm 1.5^\circ$ . This was considered acceptable without actuation compensation.

The discrepancy was believed primarily from three major sources: the bending errors on the  $\theta$  value, and the assembling errors on the  $L$  and  $D$  values. Three calibration coefficients were introduced:  $C_\theta$ ,  $C_L$  and  $C_D$ . Then  $C_\theta\theta$  would be the actual bending angle when  $\theta$  is instructed.  $C_LL$  and  $C_DD$  would be the actual  $L$  and  $D$  values.

Using the measurements by the tracker and the kinematics in equation (4), an optimization could be formulated as in equation (19), involving  $C_\theta$ ,  $C_L$  and  $C_D$ . Then the *fminsearch* function in Matlab was used to solve this optimization to obtain the coefficients:  $C_\theta = 0.8698$ ,  $C_L = 1.0772$  and  $C_D = 1.0265$ :

$$\min_{C_\theta, C_L, C_D} \sum \|\tilde{\mathbf{p}}_{\text{measure}} - {}^b\mathbf{T}_f(C_\theta, C_L, C_D)\tilde{\mathbf{p}}_{\text{marker}}\| \quad (19)$$

where  $\tilde{\mathbf{p}}_{\text{measure}} = [\mathbf{p}_{\text{measure}}^T \ 1]^T$  is the homogeneous vector for the measured marker positions  $\mathbf{p}_{\text{measure}}$ ,  $\tilde{\mathbf{p}}_{\text{marker}} =$

$[\mathbf{p}_{\text{marker}}^T \ 1]^T$ ,  $\mathbf{p}_{\text{marker}}$  is the marker's position in  $\{f\}$ , and  ${}^b\mathbf{T}_f$  ( $C_\theta, C_L, C_D$ ) is from equation (4) with the coefficients of  $C_\theta$ ,  $C_L$  and  $C_D$  substituted.

Then the actuation compensation for the CurviPicker could be expressed as in equation (20):

$$\tilde{\theta} = \theta / C_\theta \quad (20)$$

where  $\tilde{\theta}$  is the commanded value for a desired  $\theta$  value.

The  $L$  and  $D$  values in the kinematics model in equation (4) are replaced by the actual values  $C_LL$  and  $C_DD$ .

It is assumed that the  $\varphi$  and  $h$  joints do not need calibration since the flexible shaft cannot be twisted or compressed.

The CurviPicker was then instructed to nine positions with the compensation implemented. In these nine positions,  $h$  is set at 110 mm while the  $\varphi$  is set to 0. These nine positions are chosen distinct from the 72 measured positions before calibration to verify the validity of the calibrated parameters in the whole workspace of the CurviPicker. The results are shown in Figure 6 (b) with the numbering of these positions. The errors in the XYZ directions are within  $\pm 2$  mm. To be noted,

the errors are steady-status errors. The tip's positioning errors could be bigger during the rapid movements.

The position errors might come from many aspects, e.g. the segments' non-ideal bending, backlash in the actuation assembly, friction in transmission and effect of gravity, etc. In order to further investigate the sources of the steady-status errors, an error analysis was performed using the Jacobian matrix of the CurviPicker from equation (8). Errors from the joint space are mapped to the task space through the Jacobian in equation (8). Since the CurviPicker's main structure is the inverted dual continuum mechanism, particular attention was directed to  $q_1$  and  $q_2$ .

As shown in Figure 7, the errors ranged from  $-0.1$  mm to  $+0.1$  mm on  $q_1$  and  $q_2$  are mapped to the positioning errors of the end effector at Position #1 which is indicated in Figure 6 (b). The errors in the task space are as big as approximately 3 mm stemmed from the 0.1 mm actuation errors in the joint space. Since the actuation errors within 0.1 mm are highly possible in the current cost-effective construction of the CurviPicker, the total positioning errors in Figure 6 (c) is considered mainly from the actuators. These actuation errors led to bigger positioning errors, propagating through the CurviPicker's structure. Finer actuators (more accurate racks, pinions and servo motors) could be used in a future study to improve the performance of the CurviPicker.

There also exists friction between the flexible shaft and the CurviPicker's arm. In the motion calibration where steady-state positioning errors were recorded, the friction was not found to affect the positioning accuracy. At least the caused errors have been included into the actuation compensation parameters. However, the disturbance caused by the insertion and rotation of the flexible shaft certainly plays a role in causing dynamic positioning errors during the movements of the CurviPicker. Due to the limited access to advanced measurement equipment, these dynamic errors were not recorded. Such analyses and subsequent efforts of reducing the vibrations as well as increasing the dynamic positioning accuracy will constitute a future study.

## 5.2 Trajectory planning and pick-and-Place tests

With the motion calibrations/compensations implemented, the CurviPicker was instructed to perform a set of pick-and-place tests with two types of objects: pill packs and 100-gram weights, as shown in Figure 8 and the multimedia extension.

The pick-and-place tasks are currently conducted in a teaching mode for proof of concept. First, the CurviPicker is

**Figure 7** Errors from the joint space are mapped to the task space for  $\Delta q_1, \Delta q_2 \in [-0.1, 0.1]$  mm at Position #1 from Figure 6 (b)

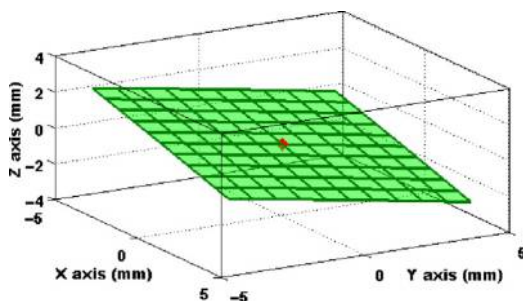
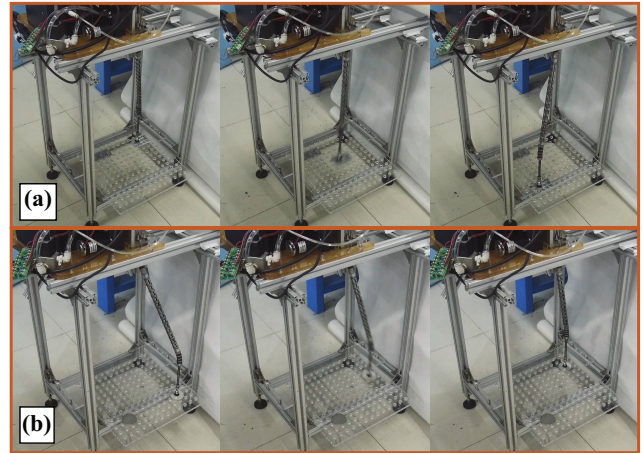


**Figure 8** Pick-and-place tests of the CurviPicker



**Notes:** (a) Pill packs; (b) 100-gram weights

moved to the picking position by nudging the configuration variables ( $\theta$ ,  $\delta$ ,  $\varphi$  and  $h$ ). Actuation lengths  $q_i$  are obtained according to equation (6). Then the CurviPicker is moved to the placing position in the same manner. With the actuation variables obtained at the initial and target positions, the trajectory planning is conducted in the joint space to move the CurviPicker from one pose to another. The reason for using trajectory planning in the joint space is that it is considered the intermediate poses of the CurviPicker are less critical as long as it reaches the picking and placing positions without interfering with other work pieces.

The CurviPicker's servomotors are controlled by the digital drivers (IS620PS1R6I from Inovance Inc., Shenzhen, China). They are low-cost ones, selected to achieve affordability. In the CANOpen protocol, they only support the simplest joint level interpolation via a trapezoidal velocity profile. Limited by the motion control mode supported by the driver, the trajectory planning is carried out in a straightforward way as follows.

Regarding the three servomotors for  $q_1$ ,  $q_2$  and  $\varphi$ , initial and target positions are firstly used to calculate the top velocity  $\tilde{v}_{top}$  and the desired acceleration  $\tilde{a}$  as in (21), assuming a period of  $t_T$  and a pure acceleration-deceleration pattern. Then the initial and target positions together with the acceleration, the top velocity and the execution time  $t_T$  are sent to the motor drivers via the CAN bus.

The pure acceleration-deceleration motion pattern requires the lowest acceleration for the same amount of movement distance during the same amount of execution time. Therefore, it might introduce fewer disturbances to reduce the vibrations of the CurviPicker, given the solely available motion mode under the trapezoidal velocity profile.

$$\tilde{v}_{top} = 2(\tilde{q}_t - \tilde{q}_{initial})/t_T \quad \text{and} \quad \tilde{a} = \pm 2\tilde{v}_{top}/t_T \quad (21)$$

where  $\tilde{v}_{top}$ ,  $\tilde{a}$ ,  $\tilde{q}_{initial}$  and  $\tilde{q}_t$  stands for the top velocity, the acceleration, the initial and the target positions of  $q_1$ ,  $q_2$  and  $\varphi$  respectively.

Regarding the servomotor for  $h$ , the motor should always lift and lower the suction cup sequentially for a pick-and-place

task. Within the same amount of time  $t_T$ , the suction cup reaches the highest point  $h_{high}$  at time  $kt_T$  ( $0 < k < 1$ ). Since the CurviPicker's motors are identical, the top velocity  $|\dot{h}_{top}|$  of the  $h$  motor is set equal to the maximum of the top velocities of the three motors for  $q_1$ ,  $q_2$  and  $\varphi$  as in equation (22). The equation (22) implies that the  $h$  motor also goes through pure accelerations and decelerations. Please note that the  $h$  motor will reach both the positive top velocity  $|\dot{h}_{top}|$  and the negative top velocity  $-|\dot{h}_{top}|$  during this process, because the suction cup will ascend and descend. Thus the absolute value of  $\dot{h}_{top}$  is used in equation (22). With  $k$  and  $|\dot{h}_{top}|$  solved from equation (22), the accelerations and decelerations for the  $h$  motor could be obtained as in equation (23) for the first half and the second half of the execution time  $t_T$ :

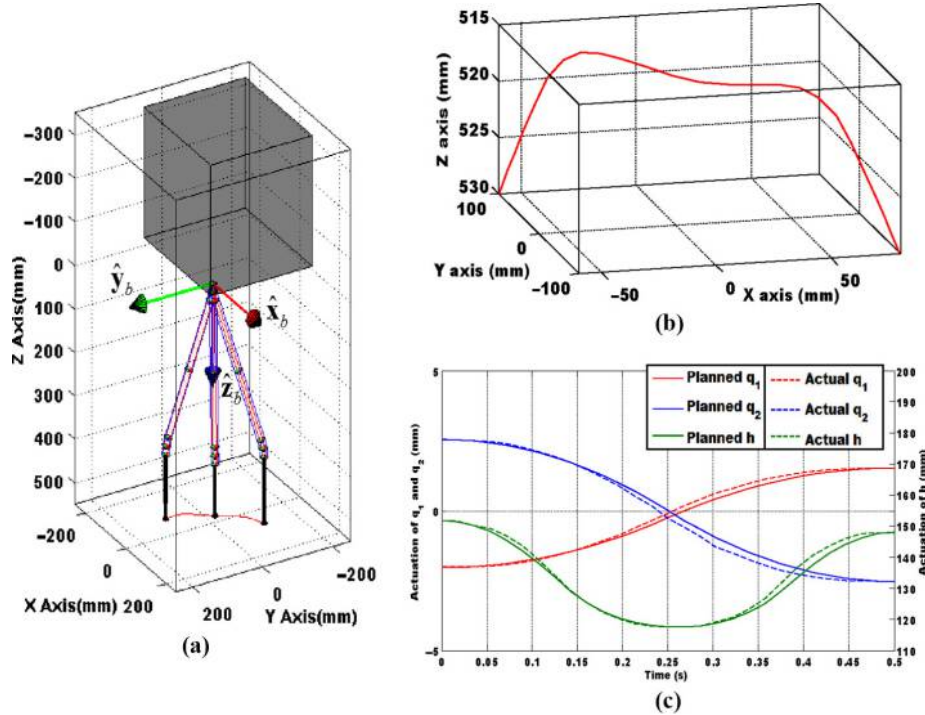
$$\frac{2(h_{initial} - h_{high})}{kt_T} = \frac{2(h_t - h_{high})}{(1-k)t_T} = |\dot{h}_{top}| = \max(|\tilde{v}_{top}|) \quad (22)$$

where  $h_{initial}$  and  $h_t$  stands for the initial and the target positions of  $h$ . Please note that  $h_{high}$  is numerically smaller than  $h_{initial}$  and  $h_t$  due to the definition of  $h$  as in Figure 2.

$$h(t) = \begin{cases} \pm 2|\dot{h}_{top}|/kt_T, & 0 \leq t \leq kt_T \\ \pm 2|\dot{h}_{top}|/(1-k)t_T, & (1-k)t_T < t \leq t_T \end{cases} \quad (23)$$

A simulation of moving the suction cup from a position  ${}^b\mathbf{p}_1 = [80 \ -100 \ 530]^T$  mm to  ${}^b\mathbf{p}_2 = [-60 \ 100 \ 530]^T$  mm within execution time  $t_T$  of 0.5 seconds is shown in Figure 9 (a).

**Figure 9** Trajectory planning of the CurviPicker



**Notes:** (a) The poses; (b) the trajectory of the suction cup; (c) planned and actual trajectories of the actuators

During this movement,  $\varphi$  is kept at  $0^\circ$ . The trajectory of the suction cup is shown in Figure 9 (b) with the planned and the actual trajectories of the actuators shown in Figure 9 (c).

As shown in Figure 8 and the multimedia extension, the CurviPicker could handle the pill packs (weight: 7 g) and the metal blocks (weight: 100 g) in a consistent manner. This weight handling range is suitable for many sortable objects for packaging, such as candy bars and snacks. During these pick-and-place tasks, the control signal for the solenoid valve was sent via a digital I/O in the embedded controller.

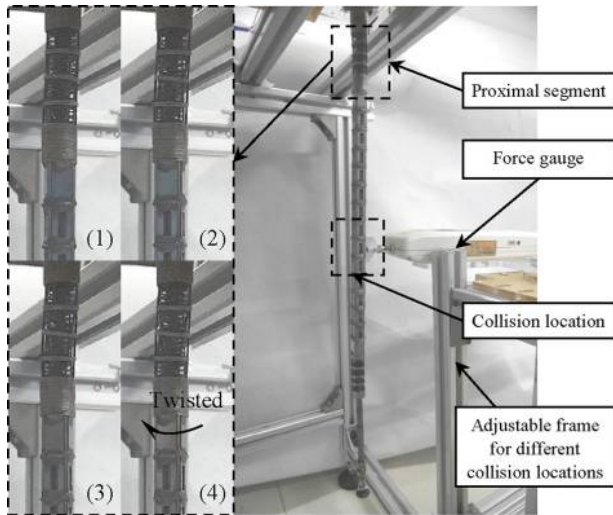
With the time  $t_T$  set to 0.5 seconds, all the objects could be picked and placed with acceptable positioning accuracy. The position errors were not quantified using the tracker since the tracker does not have such a dynamic tracking feature quick enough.

When the time  $t_T$  is set to 0.4 seconds, the CurviPicker starts to vibrate while handling the 100-gram weights. Hence, the time  $t_T$  at 0.5 s is recommended. This is equivalent to a CPM (Cycle per Minute) number of 60.

### 5.3 Safety tests

The CurviPicker possesses inherent flexibility that leads to compliant safe interactions with nearby workers. A set of experiments were hence carried out to verify the safety feature of the CurviPicker. The experimental setup is shown in Figure 10.

The CurviPicker was instructed to move from configuration #1 ( $\theta = 2\pi/15$ ,  $\delta = \pi/2$ ,  $h = 110$  mm and  $\varphi = 0$ ) to configuration #2 ( $\theta = 2\pi/15$ ,  $\delta = -\pi/2$ ,  $h = 110$  mm and  $\varphi = 0$ ) with the execution time  $t_T$  set for 0.5 seconds. A digital

**Figure 10** Experimental setup for measuring the collision forces

**Note:** (1) to (4) the PS was twisted during the collision

force gauge (HF-100 from Tripod Instrument Manufacturing Co. Ltd, Wenzhou, China) was fixed at several different positions such that the tip positions of the gauge will collide with the CurviPicker at different locations. The gauge's tip positions are listed as in Table II. In Figure 10, the tip position of the gauge is located at  $[0\ 0\ 200]^T$  (designated in the coordinate of  $\{b\}$ ). The linear velocities at the contacting positions on the CurviPicker before collision are calculated according to the applied path planning and are listed in Table II. These velocities at the positions further away from the CurviPicker's base increase accordingly. Please note that the listed velocities before collision may slightly differ from the actual values because the controller does not drive the CurviPicker completely as planned and the gauge tip position was not exactly located.

The force gauge would collide with the CurviPicker. Peak force measurement mode of the force gauge was used to record the collision force. The measured collision forces are listed in Table II. The collision process could also be seen in Figure 10 and the multimedia extension. From the zoomed view, it is clear that the CurviPicker's PS was twisted when the force gauge blocked the arm's movements.

It can be observed from Table II that the collision forces decrease with respect to the increased distance from the colliding position to the base of the CurviPicker's continuum arm. This is consistent with the fact that the CurviPicker's PS could only provide a certain amount of torque to drive the CurviPicker's arm. The maximal value of this torque depends on the torsional stability of the CurviPicker's PS. When the external resistance is bigger than this torque, the PS will start twisting (buckling in a torsional way). Then when the collision position is further away from the arm's base, a smaller force would be able to stop the CurviPicker, even though higher velocities occurred at these colliding positions.

The measured collision force is mostly less than 20 N, which is substantially lower than the tolerable contact force of 50 N from a manipulator as presented in (Yamada *et al.*, 1997). Furthermore, the CurviPicker resume its operation after the collisions. The CurviPicker is hence considered safe to work with, even in the absence of protection cages.

## 6. Conclusions and future work

The paper presents the design, kinematics, construction and experimentation of the CurviPicker, the first continuum robot for low-load medium-speed pick-and-place tasks in a safe and affordable way. It realizes the Schönflies motions using the inverted dual continuum mechanism, providing an alternative approach that is different from rigid-linked robots.

Through modeling and experimental characterizations, the CurviPicker has been shown easy to control due to its simple kinematics. Its structural compliance makes it safe to work with, as well as more adaptable and less sensitive to possible target picking position errors from non-ideal trajectory planning to avoid damaging the to-be-picked objects or itself.

Compared with SCARA and Delta robots commercially used in many industries, the Curvipicker presents a lower movement speed and lower positioning accuracy. However, it is proven to be easy and safe to use due to its simple kinematics and light-weighted flexible structure. The cost is affordable as well. These advantages could render the Curvipicker suitable for businesses that have relative low production throughputs but still yearn for automations.

Future works mainly include the following aspects. The translation in the vertical direction is currently realized by moving a central flexible shaft. Insertion of the flexible shaft introduces disturbances to the CurviPicker's shape. It is desired

**Table II** Measured collision forces with the CurviPicker

Gauge tip position designated in $\{b\}$ (mm)	Velocities at the contacting positions before collision (mm/s)	Measured collision force (N)			
		1	2	3	Average
$[0\ 0\ 200]^T$	596.0	20.4	19.6	19.2	19.7333
$[0\ 0\ 240]^T$	728.5	16.6	16.7	16.8	16.7000
$[0\ 0\ 280]^T$	860.9	12.7	12.6	12.6	12.6333
$[0\ 0\ 320]^T$	993.4	11.1	11.1	11.0	11.0667
$[0\ 0\ 360]^T$	1126	9.6	9.6	9.7	9.6333
$[0\ 0\ 400]^T$	1192	8.3	7.9	8.1	8.1000
$[0\ 0\ 440]^T$ *	1192	7.8	7.6	7.6	7.6667

**Note:** \*The collision occurred on the rigid sleeve of the end effector

to explore other form variations to use structural deformation to realize the vertical translation. Furthermore, the control infrastructure should be improved in the next development to allow more sophisticated path planning and vibration suppression algorithms to further increase the execution speed of the pick-and-place tasks. Elasto-dynamics models could be also incorporated to facilitate this future goal.

## References

- Angeles, J., Caro, S., Khan, W. and Morozov, A. (2006), "Kinetostatic design of an innovative Schönflies-motion generator", *Proceedings of the Institution of Mechanical Engineers, Part C: Journal of Mechanical Engineering Science*, Vol. 220, pp. 935-943.
- Burgner-Kahrs, J., Rucker, D.C. and Choset, H. (2015), "Continuum robots for medical applications: a survey", *IEEE Transactions on Robotics*, Vol. 31 No. 6, pp. 1261-1280.
- Carricato, M. (2005), "Fully isotropic Four-Degrees-of-Freedom parallel mechanisms for Schoenflies motion", *The International Journal of Robotics Research*, Vol. 24 No. 5, pp. 397-414.
- Clavel, R. (1990), "Device for the movement and positioning of an element in space", US patent application.
- Di Gregorio, R. (2004), "Determination of singularities in Delta-like manipulators", *The International Journal of Robotics Research*, Vol. 23 No. 1, pp. 89-96.
- Gogu, G. (2007), "Structural synthesis of fully-isotropic parallel robots with Schönflies motions via theory of linear transformations and evolutionary morphology", *European Journal of Mechanics - A/Solids*, Vol. 26 No. 2, pp. 242-269.
- Hannan, M.W. and Walker, I.D. (2003), "Kinematics and the implementation of an elephant's trunk manipulator and other continuum style robots", *Journal of Robotic Systems*, Vol. 20 No. 2, pp. 45-63.
- Krut, S., Company, O., Nabat, V. and Pierrot, F. (2006), "Heli4: a parallel robot for scara motions with a very compact traveling plate and a symmetrical design", *IEEE/RSJ International Conference on Intelligent Robots and Systems (IROS)*, October 9-15, Beijing, pp. 1656-1661.
- Li, Z. and Du, R. (2013), "Design and analysis of a bio-inspired wire-driven multi-section flexible robot", *International Journal of Advanced Robotic Systems*, Vol. 10 No. 4, pp. 209-219.
- Li, Z., Lou, Y., Zhang, Y., Liao, B. and Li, Z. (2013), "Type synthesis, kinematic analysis, and optimal design of a novel class of Schönflies-motion parallel manipulators", *IEEE Transactions on Automation Science and Engineering*, Vol. 10, pp. 674-686.
- Li, Z., Ren, H., Chiu, P.W.Y., Du, R. and Yu, H. (2016), "A novel constrained wire-driven flexible mechanism and its kinematic analysis", *Mechanism and Machine Theory*, Vol. 95, pp. 59-75.
- Miller, K. (2004), "Optimal design and modeling of spatial parallel manipulators", *The International Journal of Robotics Research*, Vol. 23 No. 2, pp. 127-140.
- Pernette, E., Henein, S., Magnani, I. and Clavel, R. (1997), "Design of parallel robots in microrobotics", *Robotica*, Vol. 15 No. 4, pp. 417-420.
- Pierrot, F. and Company, O. (1999), "H4: a new family of 4-DOF parallel robots", *IEEE/ASME International Conference on Advanced Intelligent Mechatronics (AIM)*, September 19-23, Atlanta, GA, pp. 508-513.
- Pierrot, F., Nabat, V., Company, O., Krut, S. and Poignet, P. (2009), "Optimal design of a 4-DOF parallel manipulator: from academia to industry", *IEEE Transactions on Robotics*, Vol. 25 No. 2, pp. 213-224.
- Richard, P.-L., Gosselin, C.M. and Kong, X. (2006), "Kinematic analysis and prototyping of a partially decoupled 4-DOF 3T1R parallel manipulator", *Journal of Mechanical Design*, Vol. 129 No. 6, pp. 611-616.
- Stock, M. and Miller, K. (2003), "Optimal kinematic design of spatial parallel manipulators: application to linear Delta robot", *Journal of Mechanical Design*, Vol. 125 No. 2, pp. 292-301.
- Tobushi, H., Furuichi, Y., Sakuragi, T. and Sugimoto, Y. (2009), "Bending fatigue properties of a superelastic thin tube and a high-elastic thin wire of TiNi alloy", *Materials Transactions*, Vol. 50 No. 8, pp. 2043-2049.
- Trivedi, D., Rahn, C.D., Kier, W.M. and Walker, I.D. (2008), "Soft robotics: biological inspiration, state of the art, and future research", *Applied Bionics and Biomechanics*, Vol. 5 No. 3, pp. 99-117.
- Vischer, P. and Clavel, R. (1998), "Kinematic calibration of the parallel delta robot", *Robotica*, Vol. 16 No. 2, pp. 207-218.
- Walker, I.D. (2013), "Continuous backbone 'continuum' robot manipulators", *ISRN Robotics*, Vol. 2013, pp. 1-19.
- Webster, R.J. and Jones, B.A. (2010), "Design and kinematic modeling of constant curvature continuum robots: a review", *International Journal of Robotics Research*, Vol. 29 No. 13, pp. 1661-1683.
- Wu, G., Bai, S. and Hjørnet, P. (2015), "Parametric optimal design of a parallel Schönflies-motion robot under pick-and-place trajectory constraints", *IEEE/RSJ International Conference on Intelligent Robots and Systems (IROS)*, September 28 - October 2, Hamburg, pp. 3158-3163.
- Xu, K. and Simaan, N. (2006), "Actuation compensation for flexible surgical snake-like robots with redundant remote actuation", *IEEE International Conference on Robotics and Automation (ICRA)*, (May), Orlando, FL, pp. 4148-4154.
- Xu, K. and Simaan, N. (2008), "An investigation of the intrinsic force sensing capabilities of continuum robots", *IEEE Transactions on Robotics*, Vol. 24 No. 3, pp. 576-587.
- Xu, K., Fu, M. and Zhao, J. (2014), "An experimental kinematic comparison between continuum manipulators with structural variations", *IEEE International Conference on Robotics and Automation (ICRA)*, May 31-June 7, Hong Kong, pp. 3258-3264.
- Xu, K., Zhao, J. and Fu, M. (2015), "Development of the SJTU unfoldable robotic system (SURS) for single port laparoscopy", *IEEE/ASME Transactions on Mechatronics*, Vol. 20 No. 5, pp. 2133-2145.
- Yamada, Y., Hirasawa, Y., Huang, S., Umetani, Y. and Suita, K. (1997), "Human-Robot contact in the safeguarding space", *IEEE/ASME Transactions on Mechatronics*, Vol. 2 No. 4, pp. 230-236.

- Yang, J., Pitarch, E.P., Potratz, J., Beck, S. and Abdel-Malek, K. (2006), "Synthesis and analysis of a flexible elephant trunk robot", *Advanced Robotics*, Vol. 20 No. 6, pp. 631-659.
- Zhang, L. and Song, Y. (2011), "Optimal design of the Delta robot based on dynamics", *IEEE International Conference on Robotics and Automation (ICRA)*, (9-13 May), Shanghai, pp. 336-341.

- Zhang, L., Mei, J., Zhao, X. and Huang, T. (2012), "Dimensional synthesis of the delta robot using transmission angle constraints", *Robotica*, Vol. 30 No. 3, pp. 343-349.

**Corresponding author**

**Kai Xu** can be contacted at: [k.xu@sjtu.edu.cn](mailto:k.xu@sjtu.edu.cn)